



The modeling and synthesis of nanodiamonds by laser ablation of graphite and diamond-like carbon in liquid-confined ambient

L. Basso^{1,2} · F. Gorrini^{1,2} · N. Bazzanella¹ · M. Cazzanelli² · C. Dorigoni² · A. Bifone² · A. Miotello¹

Received: 29 September 2017 / Accepted: 16 December 2017 / Published online: 29 December 2017
© Springer-Verlag GmbH Germany, part of Springer Nature 2017

Abstract

Nanodiamonds have attracted considerable interest for their potential applications in quantum computation, sensing, and bioimaging. However, synthesis of nanodiamonds typically requires high pressures and temperatures, and is still a challenge. Here, we demonstrate production of nanodiamonds by pulsed laser ablation of graphite and diamond-like carbon in water. Importantly, this technique enables production of nanocrystalline diamonds at room temperature and standard pressure conditions. Moreover, we propose a method for the purification of nanodiamonds from graphitic and amorphous carbon phases that do not require strong acids and harsh chemical conditions. Finally, we present a thermodynamic model that describes the formation of nanodiamonds during pulsed laser ablation. We show that synthesis of the crystalline phase is driven by a graphite–liquid–diamond transition process that occurs at the extreme thermodynamic conditions reached inside the ablation plume.

1 Introduction

Nanodiamonds (NDs) attracted a great interest and consequent active research, because they maintain most of the superior properties of bulk diamond and transfer them at the nanoscale. These properties include high hardness, high thermal conductivity, chemical stability, biocompatibility, and controllable surface structure [1]. This makes NDs promising for a variety of applications in different fields [2–4]. Of particular interest are NDs containing nitrogen-vacancy (NV) center. Indeed, the spin-dependent photoluminescence of this point defect [5] allows the detection of external perturbations, such as magnetic fields, suggesting the uses of NV-enriched NDs as nanoproboscopes [6]. A number of techniques have been proposed for the production of NDs, including milling of bulk diamond, detonation, and high-temperature high-pressure synthesis [1, 7, 8]. Indeed, the diamond phase requires very high pressures and temperatures, respectively, of the order of GPa and thousands

of Kelvin, for its formation [9]. Here, we propose a method for the preparation of NDs by pulsed laser ablation of carbon targets immersed in water. The main advantage of this technique is that it enables the synthesis of NDs at room temperature and standard pressure conditions. We propose a thermodynamic model explaining the formation mechanism of NDs under the transient physical conditions in the ablation plume. Finally, we describe a simple physico-chemical cleaning method of NDs, needed for the removal of graphitic byproducts of the ablation process. Moreover, a second way to obtain NDs is followed: it consists on the pulsed laser irradiation of a diamond-like carbon (DLC) film immersed in water. DLC films are synthesized by the standard pulsed laser deposition (PLD) of pyrolytic graphite in vacuum conditions. Also in this case, a model for the synthesis of NDs is described.

2 Materials and methods

2.1 Ablation of graphite in water

The ablation of the pyrolytic graphite target in ultra-pure water was performed using a Lambda Physik LPX220i KrF excimer laser with a wavelength of 248 nm and pulse duration of 20 ns. Laser energy used was in the interval 500–600 mJ per pulse, with a repetition rate of 10 Hz. The

✉ L. Basso
luca.basso-1@unitn.it

¹ Dipartimento di Fisica, Università Degli Studi di Trento, Via Sommarive 14, 38123 Povo, TN, Italy

² Center for Neuroscience and Cognitive Systems, Istituto Italiano di Tecnologia, Corso Bettini 31, 38068 Rovereto, TN, Italy

experimental setup is shown schematically in Fig. 1. The laser beam was focused on the graphite target surface, using a lens with a 400 mm focal length. A lens with such relatively long focal length was used to increase the distance between the objective and the water surface, thus avoiding deposition of water on the lenses during irradiation. The laser beam was focused to a spot of $0.73 \pm 0.05 \text{ mm}^2$ (obtained by measuring the spot size on the target surface by scanning electron microscopy after one pulse irradiation), and the laser fluence was varied in the range between ~ 50 and $\sim 60 \text{ J cm}^{-2}$, where the energy losses of $\sim 25\%$ due to the presence of the optics are taken into account.

To reduce the splashing of water, since it brings also to the loss of the ablated particles dispersed in the liquid, a cylindrical graphite target with the top surface tilted was used, as schematically shown in Fig. 1. The thickness of the water layer above the laser focal spot was of 2–3 mm. Since the flow velocity of the plume is perpendicular to the graphite surface, this configuration reduced the sputtering of water drops during irradiation. The angle of inclination of the top surface was set to 45° . To avoid the formation and deepening on the target surface, the target was moved every 1000 pulses. To collect a sufficient amount of ablated particles, the irradiation was performed for 1 h. After ablation, the target was removed from the vial, and the water-suspended powder was slowly dried in an oven at 90°C , until complete evaporation of water.

2.2 Purification method

Many different purification methods based on selective oxidation of sp^2 carbons by gas- or liquid-phase oxidants were reported [10]. Here, to remove the graphitic byproducts and isolate NDs, the following cleaning technique was implemented. First, the ablated particles were sonicated in 2-propanol for 3 h. Then, the 2-propanol was removed by evaporation, and the powders were dispersed in a solution of concentrated hydrogen peroxide H_2O_2 in water (50% in

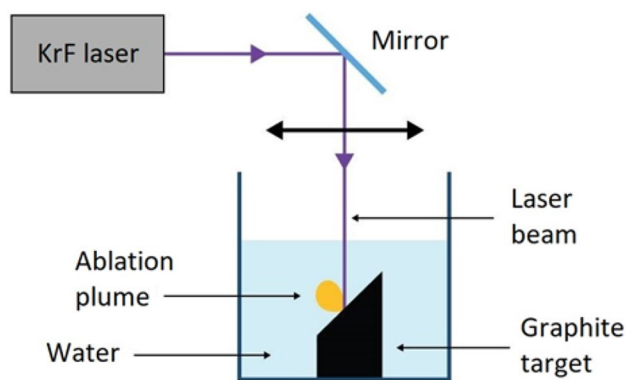


Fig. 1 Pulsed laser ablation in liquid experimental setup

weight), and irradiated by a UV lamp (wavelength of 365 nm and power intensity of 140 mW cm^{-2}) for 6 h. The ultraviolet light promotes the dissociation of hydrogen peroxide to form hydroxyl groups $\cdot\text{OH}^-$. This kind of free radicals can etch sp^2 carbons more efficiently than sp^3 carbons, due to the lower bond strength, and remove graphitic residues from the surface of NDs. After the irradiation, the water and residual H_2O_2 was evaporated, and the cleaned powders were deposited on a silicon substrate for subsequent analysis.

2.3 DLC synthesis

The diamond-like carbon (DLC) films were produced by pulsed laser deposition (PLD) of a graphite target in vacuum. The ablation of the graphite target was performed with a residual pressure inside the vacuum chamber of $1.1 \times 10^{-5} \text{ mbar}$, with the same KrF excimer laser used for the ablation in liquid. The laser beam impinged on the graphite target with an incident angle of 45° and with a spot diameter of 1 mm^2 . The graphite target was rotated during ablation, to avoid formation of a crater in the irradiation spot. Laser fluence used during deposition was of $22 \pm 1 \text{ J cm}^{-2}$. The value was chosen on the basis of the previous literature reporting increase in the fraction of sp^3 carbon atoms inside the deposited DLC film for large fluence [11]. The graphite target was placed at a distance of 7 cm from a silicon substrate. The cleaning procedure of the silicon substrate includes three subsequent cleaning steps in acetone, ethanol, and deionized water in an ultrasonic bath (10 min each) followed by a drying in a gaseous nitrogen feeble flux. The total number of pulses was 5000 with a repetition rate of 10 Hz. After deposition, the film was annealed to relax internal stresses [12]. To this end, the substrate was mounted on a heated holder, and the temperature was brought to 300°C , with a heating ramp of rate $0.1\text{--}0.2^\circ \text{C s}^{-1}$, for 1 h. Characterization of the DLC film is provided in Fig. 3c, showing the microRaman spectrum. Only one broad peak is visible at 1550 cm^{-1} , corresponding to the G peak, typical of DLC films with a high fraction of sp^3 carbon atoms. Raman spectroscopy provides a qualitative means to estimate the sp^3/sp^2 ratio by measuring the intensity ratio $I(D)/I(G)$ of the D peak and the G peak. As reported in [11], when the sp^3 fraction content becomes larger than $\sim 20\%$, the $I(D)/I(G)$ ratio drops to zero. In our case, since the D peak is not visible, we can conclude that the sp^3 fraction of carbon atoms in the DLC film is above 20%. The DLC films were deposited following the procedure reported in [11], where more qualitative analysis (such as electron energy loss spectroscopy) of the sp^3/sp^2 ratio was performed. In that work, the formation of DLC films with an sp^3 content of 80% was reported; since the deposition of the DLC film was done under same experimental conditions, we assume that the sp^3 fraction is the same of [11]. The deposited film was 140 nm thick, as shown in the SEM

image of its side wide, given in the inset of Fig. 3c. The DLC films were then immersed in 2–3 mm of deionized water and irradiated with a single shot of the KrF laser, focused with a large spot size, of $13.3 \pm 0.7 \text{ mm}^2$, to have a small laser fluence of $0.76 \pm 0.05 \text{ J cm}^{-2}$.

3 Experimental result

The samples were characterized with a multi-technique approach. The external morphology of the samples was studied by scanning electron microscopy (SEM), using a JSM-7001F FEG-SEM, while the chemical composition of the nanoparticles was investigated by energy dispersive X-ray spectroscopy (EDXS). Moreover, microRaman spectroscopy was performed to get insight in the hybridization state of the carbon atoms, using a Jobin Yvon LabRAM ARAMIS spectrometer with a 532 nm as exciting wavelength.

3.1 NDs obtained through ablation of graphite in water

A typical SEM image of the ablated particles after purification is shown in Fig. 2a, while Fig. 2b presents the corresponding EDXS spectrum. Clustered crystallites of the size of the order of hundreds of nanometers, attributed to ND agglomerates, were obtained. These clusters were still embedded in what is believed to be graphite, given that the EDXS spectrum detected only the presence of carbon. The signal in EDXS spectrum of silicon comes from the substrate on which the powders were deposited, while the peak of oxygen comes from the oxidation of the surface layers of the samples.

The purified samples were analyzed with Raman spectroscopy: the spectrum is shown in Fig. 2c. The ND peak, at 1335 cm^{-1} , is shifted to higher energy with respect to bulk diamond, whose Raman peak is at 1332 cm^{-1} [13]. This is attributed to the presence of stress in the NDs, in particular compression exerted by the external graphitic matrix, that leads to an increase in the vibrational frequency of the carbon atoms [14]. The FWHM of the peak is of 45 cm^{-1} that can be explained by the compressive strain [15] or by small size of the single diamond crystallites (ultranano-crystalline range) [16]. Nevertheless, the spectrum is dominated by the *G* peak of graphite at 1580 cm^{-1} , meaning that a residual sp^2 carbon atom matrix is still present. The *D* peak, usually at 1350 cm^{-1} , is not detected: this is likely due to the small numbers of organized sixfold sp^2 carbon aromatic rings after the laser irradiation and the cleaning process [17]. The *G* peak vibrations, instead, do not require sixfold aromatic rings, and they are present also when the carbons are organized in chain structures. Moreover, the strong intensity of the *G* peak can be explained by the higher sensitivity of

visible Raman spectroscopy to the π bonds between sp^2 carbon atoms rather than the σ bonds between carbon atoms in the sp^3 hybridization [17].

3.2 NDs obtained through ablation of DLC in water

The DLC film was immersed in water and irradiated with a single laser pulse having fluence of 0.76 J cm^{-2} ; Fig. 3a, b presents the SEM images of the irradiated film at different magnification, showing nanoparticles below 100 nm size dispersed on the film. These carbon nanostructures were studied with Raman spectroscopy; the result is shown in Fig. 3d. The peak at 1337 cm^{-1} can be attributed to compressed-strained NDs, while the *G* peak is detected at 1572 cm^{-1} .

4 Thermodynamic model

The detailed discussion on the thermodynamic model explaining the formation of NDs during ablation of graphite in water is developed in [18], and, here the model is extended to DLC targets. This model is based on two peculiarities of laser ablation in liquid ambient, namely, the high cooling rate and the values of pressure and temperature that can be obtained under pulsed laser irradiation processes. In particular, the pressure is a consequence of the shockwave emission caused by laser ablation, but it is not enough to reach the so-called high-temperature high-pressure (HPHT) conditions for diamond growth. This is supported by the detailed analysis of the thermodynamic state of the plasma reported by Amans et al. [19], and by the finding of Viecelli et al. [20], that suggests a shift of the triple point of carbon phase diagram toward higher pressure when carbon nanoparticles are considered, making HPHT growth more unlikely. Moreover, through in situ X-ray diffraction, Kraus et al. observed diamond formation after shock compression of graphite (both pyrolytic and polycrystalline) after laser ablation in the nanosecond regime [21]. According to the carbon phase diagram given in Fig. 4, with the particular thermodynamic conditions of temperature (5000 K [22]) and pressure (2–4 GPa [18, 23]), the ablation mainly involves liquid carbon target, and in laser-induced phase explosion process, liquid carbon nanodroplets are emitted [24, 25]. The reported temperature of 5000 K [22] refers to the rotational temperature of C_2 diatomic molecules, mainly related to rigid movement of the molecule [19]. However, the rotational temperature is drifted by collisions between ablated molecules [26], and for this reason, despite thermodynamic equilibrium is not reached inside the plume, rotational temperature can be correlated to kinetic temperature of heavy species. When the temperature of the plume starts to decrease, also because of the water environment, the liquid carbon returns to the

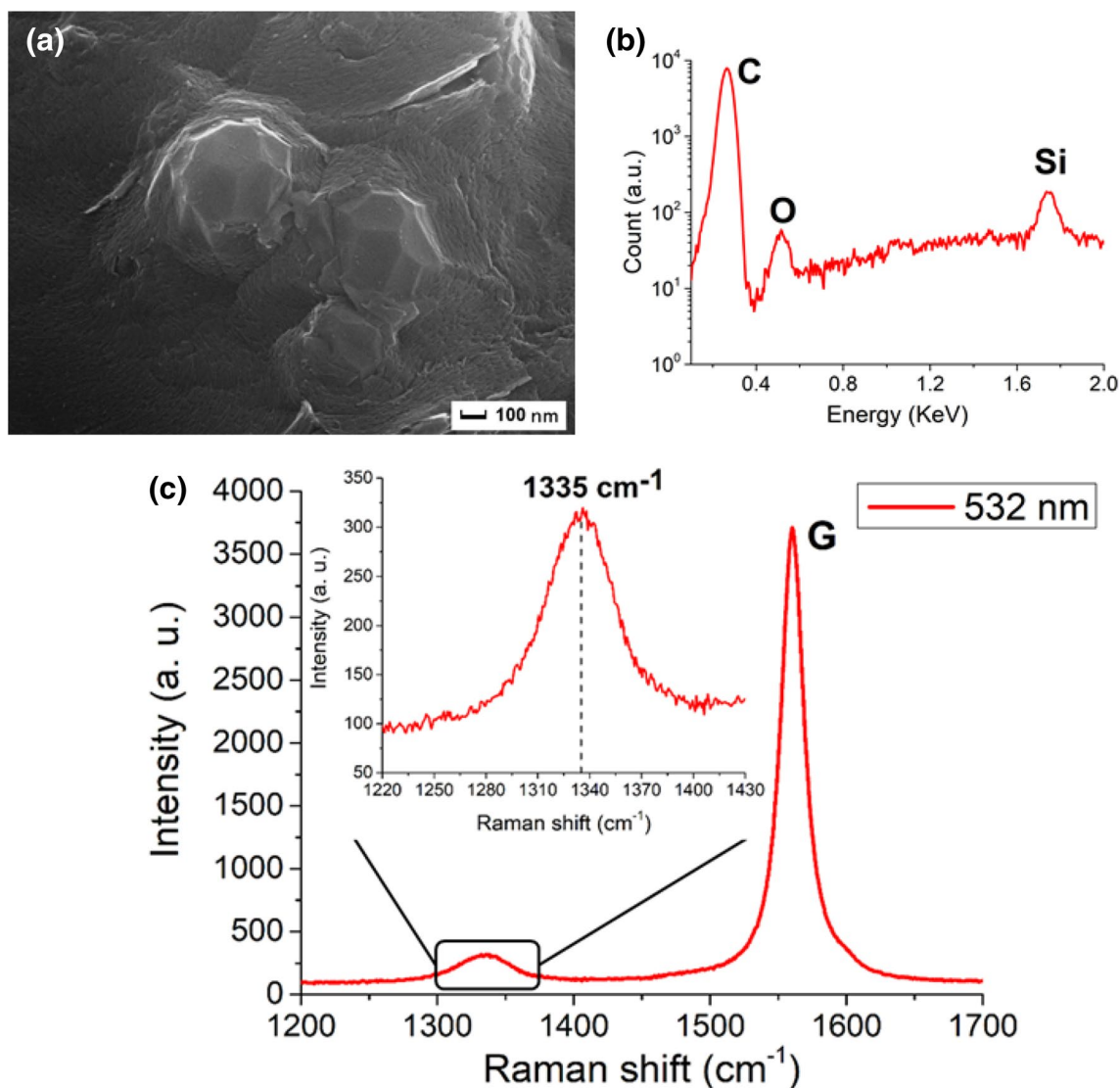


Fig. 2 **a** SEM image of a sample obtained with pulsed laser ablation of graphite in water, after removal of non-diamond phase of carbon, showing a multicrystalline particle of dimension less than 1 μm . **b** Typical EDXS spectrum of the nanoparticles: the peak of carbon is at 0.27 keV. In addition, the peaks of silicon at 1.74 keV and of oxygen at 0.52 keV are detected. They come from the substrate on which

the particles are deposited and from the oxidized surface layers of the ablated powders, respectively. **c** Raman spectrum obtained under 532 nm excitation wavelength of purified particles. The main peak at 1580 cm^{-1} is the graphite G peak, while the peak at 1335 cm^{-1} (shown in detail in the inset) is attributed to compressive-strained NDs

solid state. The phase in which it solidifies is determined by the cooling rate that can be 10^{10} – 10^{11} K s^{-1} for nano-second laser pulses. When the liquid carbon atoms enter a supercooling regime, the system is out of thermodynamic equilibrium, and the separation between the graphite-phase and the diamond-phase regions in the carbon phase diagram is no longer well defined, as the one described by the equilibrium phase diagram in Fig. 4. The system then enters in a region, schematized by the enlarged dashed red arrow in Fig. 4, in which diamond phase is formed as metastable phase. This condition allows for the nucleation of NDs as a metastable phase inside the plume, where the liquid carbon

clusters act as nucleation seeds. The transition to the stable form of carbon, namely, graphite, is prevented by the rapid cooling rate: the metastable phase is literally frozen under the action of the undercooling. Finally, when pressure drops, only graphite phase is formed. The duration of the shockwave-induced high-pressure state, namely, the time interval in which diamond phase forms, is estimated to be twice the duration of the laser pulse [23, 27]. After that, only sp^2 structures forms around nanodiamonds, thus requiring purification of the samples.

The most important parameter for the synthesis of NDs is the state of undercooling that allows the formation of

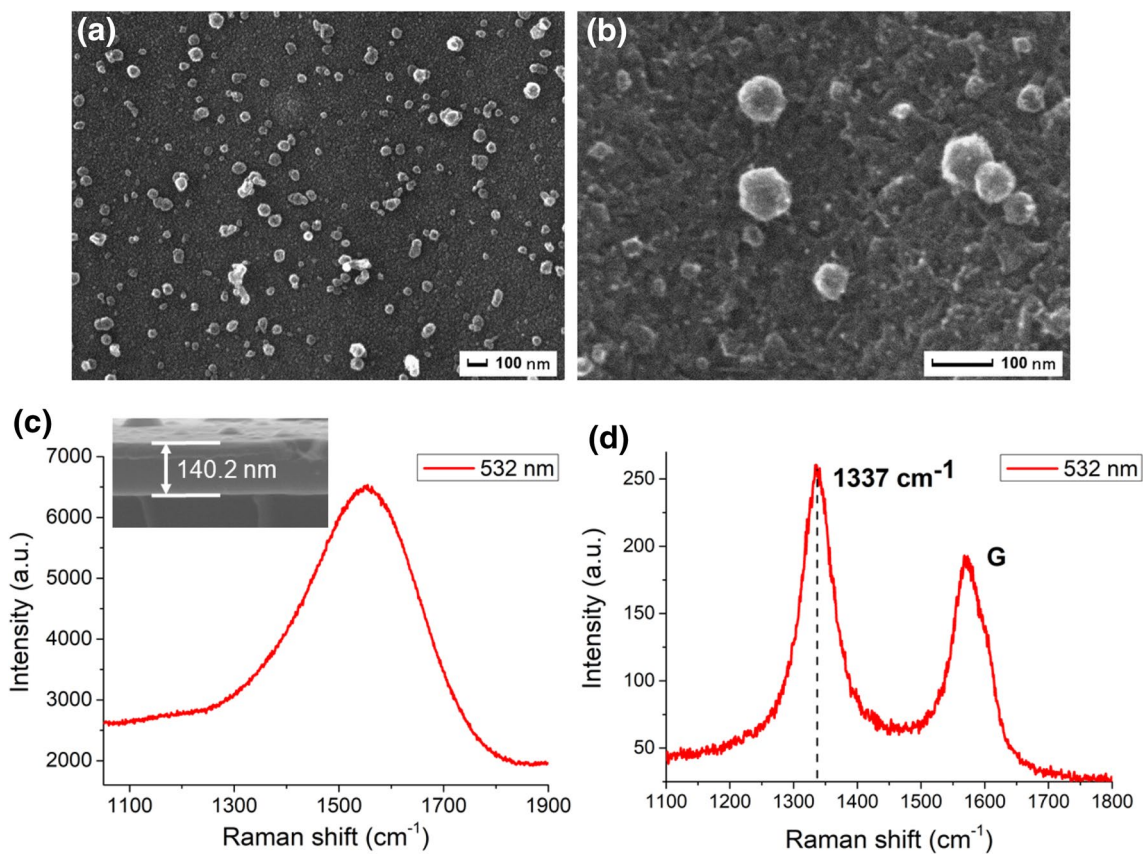


Fig. 3 **a, b** Shows two SEM images of the irradiated DLC film with a fluence of 0.76 J cm^{-2} at different magnifications; nanoparticles below 100 nm size are dispersed on the carbon film. **c** Raman spectrum of the initial DLC film obtained under 532 nm excitation wave-

length: only a broad peak at 1550 cm^{-1} is detected. **d** Raman spectrum of the irradiated film, under same excitation condition, showing the G peak at 1572 cm^{-1} , and the peak of the NDs at 1337 cm^{-1}

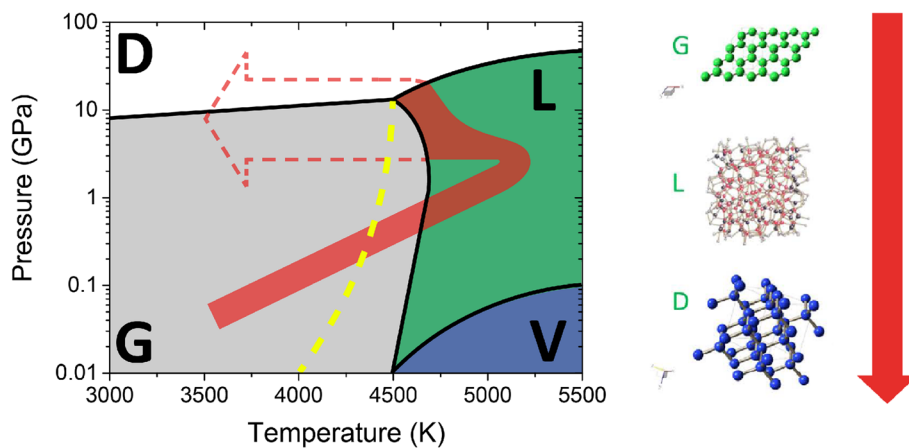


Fig. 4 Carbon phase diagram. Different colors indicate the regions in which a certain phase of carbon is thermodynamically stable: white for diamond (D), grey for graphite (G), green for liquid carbon (L), and blue for gaseous carbon (V). The yellow curve gives the melting point of DLC as a function of pressure [29]. The red arrow indicates the path for the formation of NDs during ablation of graphite in water. In the first step, the system is brought into the liquid carbon

region. Subsequently, the liquid carbon is undercooled, enabling formation and crystallization of metastable diamond phase. The dotted red arrow stresses the fact that the system is out of equilibrium and that the graphite and the diamond regions are no longer well defined as at thermodynamic equilibrium. The right side of the image represents a schematization of the multi-step process that yields the NDs

diamond phase even if the system does not enter in the diamond stable region of carbon phase diagram. This peculiar characteristic of the ablation in liquid is strongly exploited in the synthesis of NDs by ablation of DLC in water. In this case, the laser fluence is smaller, and the confinement exerted by the liquid layer is weaker, leading to a smaller increase of the pressure. Moreover, at this low laser fluence, the ablation is not relevant; therefore, the process can be referred as laser annealing. The explanation of ND formation is based on two facts. First, the DLC film that contains a large amount of sp^3 carbon atoms ($\sim 80\%$ in our case) implies that there are already clusters made by sp^3 carbon atoms in the film [28], but without a crystalline order. Second, it was demonstrated that diamond-like carbon melts at much lower temperature as compared to crystalline carbon [29]. As indicated by the yellow curve of Fig. 4 that shows the melting temperature of DLC as function of pressure, DLC melts at lower temperature compared to graphite. As a consequence, the irradiated DLC film can be melted by laser annealing using a low fluence laser pulse that would not be able to melt a graphite target. When the amorphous carbon becomes liquid, it enters in an undercooled regime, since according to carbon phase diagram, the system is in the region in which carbon atoms are in solid phase. In this undercooled state, the sp^3 carbon clusters already present in the target provide a nucleation seed for the formation of NDs at the surface of the DLC target.

Summarizing, the choice of this particular target gives two main advantages with respect to graphite. First, the system enters in an undercooling state after irradiation with a less energetic laser pulse (0.76 J cm^{-2} vs more than 50 J cm^{-2}), thus enabling ND formation just by laser melting of the target, rather than by explosive ablation. Second, since the NDs form on the surface and are not embedded in a graphite matrix as in the graphite ablation case, a cleaning procedure for the removal of graphitic byproducts is not required.

5 Conclusions

NDs were successfully synthesized through pulsed laser ablation of graphite and DLC in water. This technique is very convenient, since it enables formation of diamond phase that usually requires extreme values of temperature and pressure, performing the experiment at standard pressure and room temperature conditions. Moreover, a liquid-phase purification technique of NDs from the non-diamond phase, in which NDs are embedded in the case of ablation of graphite, is described. This is an effective cleaning procedure, since it possesses the advantages of the liquid-phase purification techniques, namely, the high density of the oxidizer, but without harsh chemical conditions and dangerous

acidic environment. The advantages of using DLC targets in ND production are then exploited. In particular, the ND formation just occurs by laser melting of the target, rather than by explosive ablation, because of the lower melting temperature of DLC with respect to graphite. In addition, since the NDs form on the surface and are not embedded in a graphite matrix as in the graphite ablation case, a cleaning procedure for the removal of graphitic byproducts is not required. Finally, a thermodynamic model of formation of NDs by ablation of graphite and DLC in liquid is provided.

References

1. V.N. Mochalin, O. Shenderova, D. Ho, Y. Gogotsi, *Nat. Nanotechnol.* **7**, 11 (2012)
2. V.Y. Dolmatov, *Russ. Chem. Rev.* **70**, 607 (2001)
3. Q. Zhang, V.N. Mochalin, I. Neitzel, I.Y. Knoke, J. Han, C.A. Klug, J.G. Zhou, P.I. Lelkes, Y. Gogotsi, *Biomaterials* **32**, 87 (2011)
4. E.K. Chow, X.Q. Zhang, M. Chen, R. Lam, E. Robinson, H. Huang, D. Schaffer, E. Osawa, A. Goga, D. Ho, *Sci. Transl. Med.* **3**, 73ra21 (2011)
5. M.W. Doherty, N.B. Manson, P. Delaney, F. Jelezko, J. Wrachtrup, L.C. Hollenberg, *Phys. Rep.* **528**, 1 (2013)
6. D. Le Sage, K. Arai, D.R. Glenn, S.J. DeVience, L.M. Pham, L. Rahn-Lee, M.D. Lukin, A. Yacoby, A. Komeili, R.L. Walsworth, *Nature* **496**, 486 (2013)
7. K. Iakoubovskii, M.V. Baidakova, B.H. Wouters, A. Stesmans, G.J. Adriaenssens, A.Y. Vul', P.J. Grobet, *Diam. Relet. Mater.* **9**, 861 (2000)
8. C.R. Lin, D.H. Wei, M.K. Ben Dao, R.J. Chung, M.H. Chang, *Appl. Mech. Mater.* **284**, 168 (2013)
9. X.D. Ren, R. Liu, L.M. Zheng, Y.P. Ren, Z.Z. Hu, H. He, *Appl. Phys. Lett.* **107**, 141907 (2015)
10. A.M. Schrand, S.A.C. Hens, O.A. Shenderova, *Crit. Rev. Solid State Mater. Sci.* **34**, 18 (2009)
11. M. Bonelli, A.C. Ferrari, A. Fioravanti, A. Li Bassi, A. Miotello, P.M. Ossi, *Eur. Phys. J. B* **25**, 269 (2002)
12. P. Mosaner, M. Bonelli, A. Miotello, *Appl. Surf. Sci.* **208**, 561 (2003)
13. D.S. Knight, W.B. White, *J. Mater. Res.* **4**, 385 (1989)
14. S.K. Sharma, H.K. Mao, P.M. Bell, J.A. Xu, *J. Raman Spectrosc.* **16**, 350 (1985)
15. E.D. Obratsova, M. Fujii, S. Hayashi, V.L. Kuznetsov, Y.V. Butenko, A.L. Chuvilin, *Carbon* **36**, 821 (1998)
16. X.D. Ren, H.M. Yang, L.M. Zheng, S.Q. Yuan, S.X. Tang, N.F. Ren, S.D. Xu, *Appl. Phys. Lett.* **105**, 021908 (2014)
17. A.C. Ferrari, J. Robertson, *Phys. Rev. B* **61**, 14095 (2000)
18. F. Gorrini, M. Cazzanelli, N. Bazzanella, R. Edla, M. Gemmi, V. Cappello, J. David, C. Dorigoni, A. Bifone, A. Miotello, *Sci. Rep.* **6**, 35244 (2016)
19. D. Amans, M. Diouf, J. Lam, G. Ledoux, C. Dujardin, *J. Colloid Interface Sci* **489**, 114 (2017)
20. J.A. Viecelli, S. Bastea, J.N. Glosli, F.H. Ree, *J. Chem. Phys.* **115**, 2730 (2001)
21. D. Kraus, A. Ravasio, M. Gauthier, D.O. Gericke, J. Vorberger, S. Frydrych, J. Helfrich, L.B. Fletcher, G. Schaumann, B. Nagler, B. Barbrel, B. Bachmann, E.J. Gamboa, S. Goede, E. Granados, G. Gregori, H.J. Lee, P. Neumayer, W. Schumaker, T. Doepfner, R.W. Falcone, S.H. Glenzer, M. Roth, *Nat. Commun.* **7**, 10970 (2016)

22. T. Sakka, K. Saito, Y.H. Ogata, *Appl. Surf. Sci.* **197**, 246 (2002)
23. R. Fabbro, J. Fournier, P. Ballard, D. Devaux, J. Virmont, *J. Appl. Phys.* **68**, 775 (1990)
24. A. Mazzi, F. Gorrini, A. Miotello, *Phys. Rev. E* **92**, 031301 (2015)
25. A.A. Ionin, S.I. Kudryashov, L.V. Seleznev, *Phys. Rev. E* **82**, 016404 (2010)
26. J. Lam, V. Motto-Ros, D. Misiak, C. Dujardin, G. Ledoux, D. Amans, *Spectrochim. Acta Part B Atom. Spectrosc.* **101**, 86 (2014)
27. L. Berthe, R. Fabbro, P. Peyre, L. Tollier, E. Bartnicki, *J. Appl. Phys.* **82**, 2826 (1997)
28. A.C. Ferrari, J. Robertson, *Philos. Trans. R. Soc. Lond. A* **362**, 2477 (2004)
29. J. Narayan, A. Bhaumik, *APL Mater.* **3**, 100702 (2015)